Princeton Plasma Physics Laboratory

PPPL-4062

PPPL-4062

Resonance and Chaotic Trajectories in Magnetic Field Reversed Configuration

A.S. Landsman, S.A. Cohen,
M. Edelman, and G.M. Zaslavsky

April 2005

Prepared for the U.S. Department of Energy under Contract DE-AC02-76CH03073.

PPPL Report Disclaimers

Full Legal Disclaimer

Trademark Disclaimer

PPPL Report Availability

This report is posted on the U.S. Department of Energy's Princeton Plasma Physics Laboratory Publications and Reports web site in Fiscal Year 2005. The home page for PPPL Reports and Publications is: http://www.pppl.gov/pub_report/

Office of Scientific and Technical Information (OSTI):

Available electronically at: http://www.osti.gov/bridge.

Available for a processing fee to U.S. Department of Energy and its contractors, in paper from:

U.S. Department of Energy
Office of Scientific and Technical Information
P.O. Box 62
Oak Ridge, TN 37831-0062

Telephone: (865) 576-8401

Fax: (865) 576-5728

E-mail: reports@adonis.osti.gov

National Technical Information Service (NTIS):

This report is available for sale to the general public from:

U.S. Department of Commerce
National Technical Information Service
5285 Port Royal Road
Springfield, VA 22161

Telephone: (800) 553-6847

Fax: (703) 605-6900

Email: orders@ntis.fedworld.gov

Online ordering: http://www.ntis.gov/ordering.htm

Resonance and chaotic trajectories in magnetic field reversed configuration

A. S. Landsman* and S. A. Cohen

Princeton Plasma Physics Laboratory,

P.O. Box 451, Princeton, NJ 08543

M. Edelman and G.M. Zaslavsky

Courant Institute, 4 Washington Place, New York, NY 10003

Abstract

The nonlinear dynamics of a single ion in a field reversed configuration (FRC) were investigated. FRC is a toroidal fusion device which uses a specific type of magnetic field to confine ions. As a result of angular invariance, the full three dimensional Hamiltonian system can be expressed as two coupled, highly nonlinear oscillators. Due to the high nonlinearity in the equations of motion, the behavior of the system is extremely complex, showing different regimes, depending on the values of the conserved canonical angular momentum and the geometry of the fusion vessel. Perturbation theory and averaging were used to derive the unperturbed Hamiltonian and frequencies of the two degrees of freedom. The derived equations were then used to find resonances and compare to Poincare surface-of-section plots. A regime was found where the nonlinear resonances were clearly separated by KAM curves. The structure of the observed island chains was explained. The condition for the destruction of KAM curves and the onset of strong chaos was derived, using Chirikov island overlap criterion, and shown qualitatively to depend both on the canonical angular momentum and geometry of the device. After a brief discussion of the adiabatic regime, the paper goes on to explore the degenerate regime that sets in at higher values of angular momenta. In this regime, the unperturbed Hamiltonian can be approximated as two uncoupled linear oscillators. In this case, the system is near-integrable, except in cases of a universal resonance, which results in large island structures, due to the smallness of nonlinear terms, which bound the resonance. The linear force constants, dominant in this regime, were derived and the geometry for a large one-to-one resonance identified. The above analysis showed good agreement with numerical simulations and was able to explain characteristic features of the dynamics.

PACS numbers: 52.55.Hc, 05.45.Pq, 05.45.Ac, 52.65.Cc, 52.20.Dq, 52.55.Ez

INTRODUCTION

The field-reversed configuration (FRC), see Figure 1, is a toroidal-shaped magnetic-field geometry that appears well-suited for confining plasmas for the purpose of the controlled, safe, steady-state production of fusion energy. [1, 2] A primary characteristic that distinguishes the FRC from most other toroidal fusion devices is that it has no toroidal magnetic field. Thus charged-particle motion in FRCs can not be approximated as being guided along magnetic field lines. For most fusion reactors, such as the tokamak, the magneto-hydrodynamic (MHD) theory [3] has been used successfully to investigate the physics at fusion-relevant regimes. It is well known [4, 5] that in the fusion-relevant regime the single-particle Hamiltonian approach presents a powerful, applicable method to understand the qualitative features of ion dynamics.

The single ion dynamics inside the FRC have equations identical to those of two strongly coupled nonlinear oscillators. The strong nonlinearities make for a very interesting system with various regimes that depend on the values of the coupling constants. Thus both, a highly nonlinear regime with a set of island chains caused by nonlinear resonances and a linear regime with a single large universal resonance caused by the intrinsic degeneracy can be observed.

Stochastic dynamics and resonances in nonlinear oscillators have been extensively studied in various cases of theoretical and practical interest [6–12]. The present paper is the first detailed study of the model of coupled resonances that are related to FRC. Using averaging methods and perturbation theory, we investigate particle dynamics in the FRC under the variation of two control parameters: geometric factor β, which is inverse elongation (or aspect ratio of the FRC in Figure 1) and dimensionless azimuthal angular momentum, P, that is conserved due to the azimuthal symmetry of the field. It is found that variation of β and P significantly affect the resonance structure and level of stochasticity.

The paper is organized as follows: In Sec. II the problem is set up and a two dimensional Hamiltonian is derived using conservation of azimuthal angular momentum, P. The derived Hamiltonian is then used to discuss possible types of particle orbits that can occur in the FRC for $P > 0$ ions. In Sec. III, the impact of P and elongation on resonance structure and stochasticity is studied using the Hamiltonian derived in Sec. II. First, the unperturbed Hamiltonian H_0 is derived using averaging methods. It is found that for certain range

of values of elongation and azimuthal angular momenta, the unperturbed Hamiltonian is sufficiently nonlinear and the perturbation sufficiently small, that KAM theory applies and a resonant island structure bounded by KAM curves is obtained. The paper then goes on to discuss the break-down of KAM theory with variation of parameters and the onset of strong chaos. The adiabatic regime, occuring in the large elongation (small β) limit, where a significant frequency separation occurs between the two degrees of freedom is also discussed. In Sec. IV, we turn to the near integrable case that occurs in the limit of higher azimuthal angular momenta. It is shown that in this limit, the unperturbed Hamiltonian has the form of two uncoupled harmonic oscillators, so that action-angle variables of a simple harmonic oscillator can be used in the Hamiltonian expansion. After explaining why the system is near-integrable at higher azimuthal angular momenta for elongation close to or less than one, we turn to the case of a large one-to-one universal resonance. It is shown that this large resonance is a consequence of intrinsic degeneracy, while the set of smaller resonances occuring at smaller azimuthal angular momenta values is a result of accidental degeneracy.

EQUATIONS OF MOTION AND ORBIT TYPES

II.A Basic equations of motion

The Hamiltonian for a nonrelativistic particle of charge q in a magnetic field is given by [13]:

$$H = \frac{1}{2}\left[(p_r - qA_r)^2 + (p_z - qA_z)^2 + \left(\frac{p_\phi}{r} - qA_\phi\right)^2\right] \tag{1}$$

Where $A_{r,z,\phi}$ are the components of the vector potential and $p_{r,z,\phi}$ are the canonical angular momenta. As a representative FRC system, a Solov'ev model [14] is used in which the plasma pressure has a linear dependence on magnetic flux Φ:

$$\Phi = rA_\phi \tag{2}$$

In this model, the magnetic flux is described by [15]:

$$\Phi = R^2 B_a \frac{r^2}{2R^2}\left(1 - \frac{r^2}{R^2} - \frac{\beta^2 z^2}{R^2}\right) \tag{3}$$

where B_a is the amplitude of the magnetic field at the center of the device at $r = z = 0$, R is the radius of the separatrix on the midplane at $z = 0$, and $2Z$ is the distance between X-points along the z-axis. Equation (3) shows a pressure profile that falls to zero at the

boundary of the device where $\Phi = 0$. From Eq. (2) and (3), we can obtain a vector potential, A_ϕ. Since the full vector potential of the FRC has only a ϕ component, we get the following expression for the vector potential:

$$\vec{A} = A_\phi \hat{\phi} = B_a \frac{r}{2} \left(1 - \frac{r^2}{R^2} - \frac{\beta^2 z^2}{R^2} \right) \hat{\phi} \tag{4}$$

where $\hat{\phi}$ is a unit vector in the azimuthal direction. Substituting the vector potential from Eq. (4) into Eq. (1), the Hamiltonian becomes:

$$H = \frac{1}{2m} \left[p_r^2 + p_z^2 + \left(\frac{p_\phi}{r} - q A_\phi \right)^2 \right] \tag{5}$$

where p_ϕ is the conserved canonical azimuthal angular momentum. Substitution of A_ϕ from Eq. (4) into Eq. (5) gives

$$H = \frac{1}{2m} \left\{ p_r^2 + p_z^2 + \left[\frac{p_\phi}{r} - br \left(1 - \frac{r^2}{R^2} - \frac{\beta^2 z^2}{R^2} \right) \right]^2 \right\} \tag{6}$$

where $b = qB_a/2$. The azimuthal angular momentum p_ϕ is conserved since there is no angular dependence in the Hamiltonian. The Hamiltonian above describes a two degree of freedom time-independent system. After scaling $r/R \to r$, $z/R \to z$, $p_r/bR \to p_r$, $p_z/bR \to p_z$ and $(m/b^2R^2)\, H \to H$, the dimensionless Hamiltonian becomes:

$$H = \frac{1}{2} \left\{ p_r^2 + p_z^2 + \left[\frac{P}{r} - r \left(1 - r^2 - \beta^2 z^2 \right) \right]^2 \right\} \tag{7}$$

where $P = p_\phi / bR^2$. The last term is a two-dimensional potential $V(r, z)$:

$$V(r, z) = \frac{1}{2} \left[\frac{P}{r} - r \left(1 - r^2 - \beta^2 z^2 \right) \right]^2 \tag{8}$$

After applying Hamiltonian equations of motion

$$\dot{q}_i = \frac{\partial H}{\partial p_i}; \qquad \dot{p}_i = -\frac{\partial H}{\partial q_i} \tag{9}$$

where q_i and p_i are the coordinate and momentum variables, we get

$$\ddot{r} + r\left(1 + 2P\right) - \frac{P^2}{r^3} - 4r^3 + 3r^5 + \beta^2 z^2 \left(4r^3 - 2r + \beta^2 z^2 r \right) = 0 \tag{10}$$

$$\ddot{z} + 2\beta^2 z \left[P - r^2 \left(1 - r^2 - \beta^2 z^2 \right) \right] = 0 \tag{11}$$

Note that the β variable can not be scaled away since it appears in Eq. (11) as a $\beta^2 z$ term, and effects the time scale of z motion relative to r motion.

From Eq. (11), the force along z is zero when $z = 0$. Given the initial condition $z = p_z = 0$, the ion will stay confined to the $z = 0$ plane, where the motion is one-dimensional and therefore integrable. The integrable motion in the $z = 0$ subspace is briefly described in the following section.

II.B Types of orbits

The possible types of orbits in the $z = 0$ subspace have been previously discussed. [16, 17] For positive values of P, there are two possible shapes for a potential well V as a function of r. It is either a double well with minima touching zero or a single raised well. Figure 2 shows different shapes of V, for various values of P in the $z = 0$ subplane. Higher values of P result in a shallower potential, see also Eq. (7), until there is a transition to a single raised potential at a critical value of $P_c = 1/4$. Figure 3 shows cross-sections of the potential as a function of r for different values of z. It can be seen that the double potential becomes shallower as $|z|$ increases, eventually turning into a single raised potential. For values of P above the critical threshold, the entire potential well becomes further raised as the ion travels towards higher absolute values of z.

To explain the different types of orbits observed, it is worth noting that the potential V in the reduced two-dimensional system is actually the kinetic energy in the ϕ direction in the full three-dimensional system. This is due to the fact that only magnetic fields are present, which exert a Lorentz force perpendicular to the direction of motion: $\vec{F} = q\vec{v} \times \vec{B}$, therefore the total kinetic energy is conserved. It follows that

$$H = \frac{1}{2m}\left[p_r^2 + p_z^2 + \left(mr\dot{\phi}\right)^2\right] \tag{12}$$

Comparing Eq. (12) with Eq. (6), it is clear that the last terms are equal. Since $r^2\dot{\phi}^2$ is proportional to V, it follows that $\dot{\phi}$ changes sign whenever the potential V touches zero (except at the transition to a single raised potential), therefore the ion reverses its angular direction of motion. Based on the types of potential described above, we can now explain the three possible types of orbits observed in the FRC for positive values of P, see Figure 4. First, there are cyclotron orbits which correspond to oscillations in one of the two wells of the double potential in the radial direction. They are unstable to displacement from the mid-

plane and therefore tend to travel to higher absolute values of z. The second type of orbits are figure-8 orbits which oscillate over the entire double potential. Since the barrier dividing the two wells exerts a repelling force, as can be shown by plotting Eq. (11) as a function of r (keeping z constant), higher energy figure-8 orbits are stable around $z = 0$ while lower energy ones, which spend more of their time transversing the barrier are unstable around $z = 0$. All double potential wells become shallower as an ion moves towards higher values of $|z|$, so that all cyclotron orbits will eventually have enough energy to cross the barrier in the double potential (for some non-zero value of z) and turn into figure-8 orbits, thus eventually feeling a restoring force towards $z = 0$. The third type of orbit is the betatron orbit, shown in Figure 2c, which corresponds to oscillations in a raised potential. It is characterized by $\dot{\phi} > 0$ at all times, which is explained by considering that the potential V never touches zero, and therefore $\dot{\phi}$ never undergoes a sign change. Betatron orbits are stable to displacements from $z = 0$.

RESONANCES AND CHAOS

III.A Averaged equations of motion

The Hamiltonian in Eq. 7 can be expanded as,

$$H = H_{r0}\left(p_r, r\right) + H_{z0}\left(p_z, z\right) + \epsilon H_1\left(r, z\right) \tag{13}$$

where $H_0 = H_{r0}\left(p_r, r\right) + H_{z0}\left(p_z, z\right)$ is the uncoupled, integrable portion of the Hamiltonian, and ϵ is the magnitude of the coupled terms. If H_1 is normalized to the same magnitude as H_0, ϵ gives the degree of perturbation to the integrable portion of the Hamiltonian, H_0. The above Hamiltonian can be expressed in action-angle variables of the uncoupled Hamiltonian, H_0.

$$H = H_{r0}\left(J_{r0}\right) + H_{z0}\left(J_{z0}\right) + \epsilon H_1\left(\vec{J_0}, \vec{\theta_0}\right) \tag{14}$$

where $\vec{J_0} = (J_{r0}, J_{z0})$ and $\vec{\theta_0} = (\theta_{r0}, \theta_{z0})$ are the conjugate action-angle variables of H_0. Actions J_{r0} and J_{z0} are the areas enclosed by the unperturbed trajectory in phase space,

$$J_{r0} = \frac{1}{2\pi}\oint p_r dr \qquad J_{z0} = \frac{1}{2\pi}\oint p_z dz \tag{15}$$

where the integrals are taken over one oscillation in their respective coordinates. H_{r0} and H_{z0} are used to evaluate p_r and p_z, respectively, used in Eq. (15). The equations of motion

can be written as

$$\dot{J}_{r0} = -\epsilon \frac{\partial H_1}{\partial \theta_{r0}}; \qquad \dot{J}_{z0} = -\epsilon \frac{\partial H_1}{\partial \theta_{z0}}; \qquad \dot{\theta}_{r0} = \omega_{r0} = \frac{\partial H_{r0}}{\partial J_{r0}}; \qquad \dot{\theta}_{z0} = \omega_{z0} = \frac{\partial H_{z0}}{\partial J_{z0}} \tag{16}$$

where ω_{r0} and ω_{z0} are the frequencies of the unperturbed Hamiltonian H_0 and $(\theta_{r0}, \theta_{z0})$ are defined using a generating function [6],

$$S = \sum_{q=r,z} \int_{q_0}^{q} p_q dq \tag{17}$$

where

$$\theta_{r0} = \frac{\partial S}{\partial J_{r0}} \qquad \theta_{z0} = \frac{\partial S}{\partial J_{z0}} \tag{18}$$

The perturbation term H_1 can be expanded in terms of action-angle variables:

$$H_1 = \sum_{l,m=-\infty}^{\infty} H_{l,m}\left(\vec{J}_0\right) exp\left(i\vec{n} \cdot \vec{\theta}_0\right) \tag{19}$$

where $\vec{n} = (l, m)$ is an integer vector. In (r, z) variables H_1 can be obtained from the Hamiltonian in Eq. (7),

$$\epsilon H_1 = -r^2\beta^2 z^2 + r^4\beta^2 z^2 + \frac{1}{2} r^2 \beta^4 z^4 \tag{20}$$

If the coupling is sufficiently small and there is sufficient nonlinearity, such that the conditions of KAM theory are satisfied, there exist a series of resonances bounded by KAM curves. The KAM curves are perturbed from the uncoupled Hamiltonian H_0 and can be obtained using perturbation theory. Resonance occurs whenever

$$s\omega_{r0} - q\omega_{z0} = 0 \tag{21}$$

where s, q are integers and ω_{r0}, ω_{z0} are given by Eq. (16). When the condition given by Eq. (21) occurs, there are slowly varying terms in the exponent of the expansion of H_1 in Eq. (19), leading to a significant perturbation in the Hamiltonian.

In the absence of resonances, the Hamiltonian given by Eq. (13) can be averaged along z and r to obtain averaged motion along r and z, respectively. This is equivalent to averaging Equation (14) over θ_{z0} to get the averaged r motion and over θ_{r0} to get the averaged z motion, with H_1 given by Eq. (19). All the angle dependent terms in H_1 will average to zero, except for the resonant terms [7, 10] After averaging Eq. (13) over z and r, we obtain $\bar{H}_r(r)$ and $\bar{H}_z(z)$, respectively, which represent averaged Hamiltonians for r and z motion,

$$\bar{H}_r(r) = H_{r0}(p_r, r) + \epsilon \langle H_1(r, z) \rangle_z \tag{22}$$

$$\bar{H}_z(z) = H_{z0}(p_z, z) + \epsilon\langle H_1(r, z)\rangle_r \tag{23}$$

Using these new Hamiltonians, and following the same procedure as before, one can obtain the new actions J_r and J_z, that would contain higher-order corrections to J_{r0} and J_{z0}. The frequencies ω_r and ω_z obtained using $\bar{H}_r(J_r)$ and $\bar{H}_z(J_z)$ can then be used to find the location of resonances, when

$$s\omega_r - q\omega_z = 0 \tag{24}$$

Here, (ω_r, ω_z) are corrections to $(\omega_{r0}, \omega_{z0})$. To find the averaged Hamiltonian along z, we need to substitute an approximate solution for the r motion into Eq. (7) The motion along r can be approximated as

$$r \approx r_h + Acos(\omega_r t) \tag{25}$$

where r_h is the midpoint of oscillation. It is found by setting the derivative of the potential in Eq. (8) equal to zero and solving for r. Eq. (25) takes the first term in the Fourier expansion of the motion along r. For $\beta^2 z^2 \ll 1$, r_h can be approximated as

$$r_h \approx \left(K_1 - K_2\beta^2 z^2\right)^{1/2} \tag{26}$$

where

$$K_1 = \frac{1}{6}(1 + C_1); \qquad K_2 = \frac{1}{6}(1 + 1/C_1); \qquad C_1 = (1 + 12P)^{\frac{1}{2}} \tag{27}$$

Substituting Eq. (25) into Eq. (7), expanding and keeping only the highest order non-oscillatory terms, we get the averaged unperturbed Hamiltonian along z:

$$\bar{H}_z \approx \frac{1}{2}p_z^2 + \frac{1}{2}\left(D_z\beta^2 z^2 + F_z\beta^4 z^4\right) \tag{28}$$

where D_z is a function of P and A, with A given by Eq. (25). The value of F_z is not dependent on P, as can be easily confirmed by expanding the potential. It follows that the magnitude of the z^4 term in Eq. (28) stays constant as P is increased. The quadratic term however, changes significantly as P is varied, which can be seen by expanding the potential given in Eq. (7).

To obtain H_{r0}, we follow a similar procedure as that used to obtain H_{z0} and approximate the motion along z as,

$$\beta z \approx Bcos(\omega_z t) \tag{29}$$

where B is the amplitude of oscillation along z. $B < 1$ for ions confined inside the FRC. It is convenient to change variables to $\triangle r = r - r_0$, where $r_0 = K_1^{1/2}$ (see Eq. (26)). Since

this is a simple coordinate shift, the momentum, p_r, is not effected by the transformation. Substituting Eq. (29) into Eq. (7), we get, after expanding the P^2/r^2 term in a series and dropping higher order and oscillatory terms,

$$\bar{H}_r \approx \frac{1}{2}p_r^2 + \frac{1}{2}\left(D_r \triangle r^2 + M_r \triangle r^3 + F_r \triangle r^4\right) \tag{30}$$

The coefficients D_r, M_r, and F_r are a function of azimuthal angular momentum P, and, in higher order, depend on B, or the amplitude of oscillation along z. To lowest order (neglecting amplitude dependent terms), the coefficients in Eq. (30) can be expressed in terms of K_1 and K_2 (see Eq. (27)) which are functions of P only. Approximate expressions for F_r and F_z as functions of K_1 and K_2 will be given in the next section, where the contribution of these terms to nonlinear resonance is discussed. The above approximations fail for low amplitude cyclotron orbits whose motion can not be expanded around $r_0 = K_1^{1/2}$. The measure of such orbits in phase-space decreases with increasing azimuthal angular momentum, P.

Eqs. (28) and (30) give approximate unperturbed averaged Hamiltonians for the z and r motion. From these equations, the actions J_z and J_r can be obtained using Eq. (15). These actions will be approximately conserved in the absence of resonances. Expressing $\bar{H}_r$ and $\bar{H}_z$ in terms of J_r and J_z, respectively, the frequencies of averaged r and z motion, given by Eq. (16), become

$$\omega_r = \frac{\partial \bar{H}_r}{\partial J_r}; \qquad \omega_z = \frac{\partial \bar{H}_z}{\partial J_z} \tag{31}$$

In the next section, the approximate dependence of $\bar{H}_r$ on J_r and $\bar{H}_z$ on J_z is derived and the frequencies ω_r, ω_z obtained for the case of "intermediate" values of P where Eqs. (28) and (30) become further simplified.

III.B Nonlinear resonances

The averaged Hamiltonians derived in the previous section can be used to find the location of nonlinear resonances. Figure 5 shows the lowest-order values of the coefficients in Eqs. (28) and (30), as a function of P for the averaged r and z motion. The higher-order amplitude dependent terms are not included since they vary with different trajectories. It can be seen that all except the fourth power coefficients are zero around $P \approx P_c$. Amplitude dependent terms make a positive contribution, shifting the coefficient curves upward and causing them to intersect the P-axis at a lower values. Since P_c denotes the transition to betatron orbits

and a typical FRC has a significant amount of figure-8 and cyclotron orbits, this range of P values can be considered as "intermediate". Thus in this intermediate range, centered around $P_i < P_c$, the fourth power terms predominate for both r and z motion. For typical ion energies used in the numerical simulations, which allow the ion to explore most of the FRC while remaining inside it, this range is around $(3/4)P_c < P < P_c$. Approximating $\bar{H}_r$ and $\bar{H}_z$ in Eqs. (30) and (28) for intermediate values of P, we get

$$\bar{H}_r \approx \frac{1}{2}p_r^2 + \frac{1}{2}F_r \triangle r^4 \tag{32}$$

$$\bar{H}_z \approx \frac{1}{2}p_z^2 + \frac{1}{2}F_z \beta^4 z^4 \tag{33}$$

It will be shown later that variations in F_r and F_z have a weak effect on the unperturbed frequencies, ω_r and ω_z, respectively. It follows that higher order terms can be dropped without having a significant effect on frequencies. After dropping higher-order amplitude dependent terms, the coefficients can be approximated as:

$$F_r \approx -2 + 15K_1 + \frac{4P}{K_1} + \frac{P^2}{K_1^3} \tag{34}$$

$$F_z \approx K_1 + 2K_2 - 4K_1K_2 - 2K_2^2 + 3K_1K_2^2 \tag{35}$$

For motion along z, the A^2 amplitude terms (obtained by substituting Eq. (25) into the Hamiltonian) make a positive contribution to quadratic and fourth power terms, and thus contribute to stability around $z = 0$. It follows that oscillations that have higher energies along r are confined closer to the midplane [17, 18]. Both K_1 and K_2 (see Eq. (27)) are less than one at intermediate values of P. Looking at Eqs. (34) and (35) or Figure 5, it can be seen that $F_r \gg \beta^4 F_z$, except at "high" values of β (close to two), corresponding to oblate geometry. Comparing Eqs. (32) and (33), it can be seen that for the same amplitudes of oscillation, the frequency of motion along r will be significantly higher than along z. Keeping in mind that for these nonlinear oscillators, the frequencies of oscillation increases with amplitude, it becomes clear that the important primary nonlinear resonances (those that have the greatest island width and can therefore be easily observed) occur when $\bar{H}_r \ll \bar{H}_z$.

Using Eqs. (32) and (33), we can now derive primary nonlinear resonances defined as:

$$\omega_z/\omega_r = s/q \tag{36}$$

where s, q are integers and ω_r, ω_z are the unperturbed frequencies.

Equations (32) and (33) have a Hamiltonian of the form:

$$H = \frac{1}{2}p^2 + \frac{1}{2}Fq^4 = E \tag{37}$$

where F and E are constants. The Action integral in this case is equal to:

$$J = \frac{2}{\pi}\int_0^{q_{max}} \left(2E - Fq^4\right)^{1/2} dq \tag{38}$$

where $q_{max} = (2E/F)^{1/4}$. Expanding the expression inside the integral using the formula

$$G\left(x_0 + \triangle x\right) = \sum_{n=0}^{\infty} G^n\left(x_0\right)\frac{\left(\triangle x\right)^n}{n!} \tag{39}$$

where $G^n\left(x_0\right)$ signifies the nth derivative of the function, we get:

$$\left(2E - Fq^4\right)^{1/2} = \sqrt{2E} - \frac{(2E)^{-1/2}}{2}Fq^4 - \sum_{n=2}^{\infty}\frac{(2E)^{(1/2-n)}}{2^n}\frac{F^n q^{4n}}{n!}\prod_{j=1}^{n-1}(2j-1) \tag{40}$$

Substituting Eq. (40) into the integral in Eq. (38), and integrating, we get an expression for J

$$J = aE^{3/4}F^{-1/4} \tag{41}$$

where a is a constant

$$a = \frac{2^{7/4}}{\pi}[1 - \frac{\sqrt{2}}{5} - \sum_{n=2}^{\infty}\frac{1}{2^n n!\,(4n+1)}\prod_{j=1}^{n-1}(2j-1)] \tag{42}$$

rearanging Eq. (41) and using Eq. (37) to get an expression for the Hamiltonian H in terms of the conserved action variable J, we get:

$$H = a^{-4/3}F^{1/3}J^{4/3} \tag{43}$$

with a defined by Eq. (42). Applying Hamilton's equation $\dot{\theta} = \omega = \partial H/\partial J$ to Eq. (43) and then substituting for J from Equation (41), we get an expression for frequency as a function of energy.

$$\omega = \frac{4}{3a}\left(HF\right)^{1/4} \tag{44}$$

To find the averaged frequencies ω_r and ω_z, F in Eq. (44) has to be replaced by F_r and $\beta^4 F_z$, respectively. Likewise, H should be replaced by $\bar{H}_r$ and $\bar{H}_z$ or H_r and H_z which are easily calculated from H at $z = 0$:

$$H_r = \frac{1}{2}p_r^2 + V\left(r, 0\right); \qquad H_z = \frac{1}{2}p_z^2 \tag{45}$$

and are close to $\bar{H}_r$ and $\bar{H}_z$ near the elliptical center of the resonance (in accordance with Birchkoff theorem) [7]. Note from Eq. (44) that ω is not sensitive to small variation in F and H, thus we were justified in dropping smaller order amplitude of oscillation dependent terms in the expressions for F_r and F_z.

From Eq. (44), we can now obtain a general criteria for nonlinear primary resonance that occurs at intermediate values of P where Eqs. (32) and (33) apply. Using the expression for frequency given by Eq. (44) and Eq. (36)

$$\frac{\bar{H}_z F_z \beta^4}{\bar{H}_r F_r} = \left(\frac{s}{q}\right)^4 \tag{46}$$

The equation shows that small changes in s/q require large changes in $\bar{H}_z/\bar{H}_r$

III.C Location of resonances and the effect of geometry

The amount of stochasticity and location of resonances is strongly affected by geometry of the fusion vessel. Eq. (46) can be used to compute the location of various nonlinear resonances and explore the effect of changes in geometry (variation in β). For example, taking $\beta = 1$ as a convinient starting point, and using Eq. (46), there is a one-to-one primary resonance around $H_z = (F_r/F_z)\, H_r$.

To find the location r of this resonance for the initial condition $p_r = z = 0$, we need to use a "high" value of total energy H, which allows the ion trajectory access to most of the vessel, while not going far outside the boundary set by $\Phi = 0$ so that the conditions under which Eq. (33) was derived are satisfied (see for example Figure 6). Starting from initial conditions $z = p_r = 0$ and using Eq. 45, we get: $H_z = \frac{1}{2}p_z^2$, $H_r = V(r, 0)$, when $t = 0$. Applying the conditions $H_r + H_z = H$ and $H_z = (F_r/F_z)\, H_r$ to express H_r in terms of the total energy, the location, r, of a one-to-one resonance at $z = p_r = 0$ is found by solving the following equation for r.

$$HF_z/\left(F_r + \beta^4 F_z\right) = V(r, 0) \tag{47}$$

Figure 7 shows one-to-one resonances close to $r \approx .58, .95$, values which agrees well with the ones obtained by solving the above equation. Lesser values of total energy H shift the location of this resonance inward towards lower values of r, while higher H shift the resonance outward. This is explained by using Eq. (46) where an increase in H would lead to proportionate increases in H_z and H_r (keeping everything else constant) and therefore an outward shift in the location of a one-to-one resonance towards higher values of $V(r, 0)$.

From Eq. (46), we can see that (keeping q constant) the number of islands s in a single resonance on Poincare p_r vs r plot increases as H_r decreases, keeping the total energy H fixed. H_r is determined by A, the amplitude of oscillation along r. Since $A = r - r_h$, where r is taken at $p_r = 0$, we expect to get an increasing number of islands corresponding to $s = \omega_z/\omega_r = 1, 2, 3...$, as A becomes smaller, or as we get closer to the midpoint of oscillation at $r = r_h$. Figures 7 and 8 show the increase of islands near the midpoint of oscillation at $r_h \approx .7$.

As can be seen in Eq. (33), F_z is multiplied by β^4, so that substituting $F_z\beta^4$ for F into Eq. (44), we can see that ω_z increases linearly with β, while ω_r which depends only on F_r and H_r is uneffected. From Eq. (46), a one-to-one resonance occurs whenever

$$\frac{H_z}{H_r} = \frac{F_r}{\beta^4 F_z} \tag{48}$$

It follows that an increase in β has a strong effect on the shift in the location of a one-to-one resonance towards higher amplitudes along r. Comparison of Figure 7 and Figure 9 shows this shift towards higher value of H_r with an increase in β. $F_r \approx \beta^4 F_z$ for high values of β (around $\beta \approx 2$), corresponding to oblate geometries. Figure 10 shows $s/q = 3/2$ resonance around $H_z = 3H_r$, close to what we would expect using Eq. (46). Increasing β will lead to a proportional increase of s, the number of islands, keeping everything else the same.

III.D Overlapping of resonances and the onset of strong chaos

The width of an island in a nonlinear resonance depends on the strength of the perturbation, ϵ (see Eq. (14)) and α, the degree of nonlinearity of the unperturbed Hamiltonian H_0. The nonlinearity α is defined as [8]

$$\alpha = \frac{J}{\omega}\left|\frac{\partial\omega}{\partial J}\right| \tag{49}$$

In terms of the unperturbed frequency ω, the width of an island is given by:

$$\frac{max\triangle\omega}{\omega} = (\epsilon\alpha)^{\frac{1}{2}} \tag{50}$$

To understand the destruction of KAM surfaces and the occurance of strong chaos, we introduce Chirikov's parameter K_c:

$$K_c = \frac{\triangle J}{\delta J} \tag{51}$$

where $\triangle J$ is the maximum width of the island chain (in action variables) and δJ is the distance between neighboring resonances. When $K_c \ll 1$, the island chains are clearly separated by KAM curves, between which the trajectories are confined. The resonances begin to overlap when $K_c > 1$, leading to an onset of strong chaos, characterized by stochastic behavior over much of the phase space. Approximating,

$$\triangle\omega = \frac{\partial\omega}{\partial J}\triangle J \tag{52}$$

$$\delta\omega = \frac{\partial\omega}{\partial J}\delta J \tag{53}$$

We can rewrite the criterion for the onset of strong chaos in terms of ω:

$$K_c = \frac{\triangle\omega}{\delta\omega} > 1 \tag{54}$$

To estimate the upper limit on K_c, lets calculate the overlap of the $q = 1$ resonances. From Eq. (36) the condition for s-resonance is $\omega_z = s\omega_r$, where ω_z and ω_r are functions of $\bar{H}_z$ and $\bar{H}_r$, respectively. Rewriting the above equation after substituting for ω_r from Eq. (44) we get,

$$\omega_z\left(\bar{H}_z\right) = s\frac{4}{3a}\left(F_r\bar{H}_r\right)^{1/4} \tag{55}$$

Where $\omega_z\left(\bar{H}_z\right)$ indicates that ω_z is a function of $\bar{H}_z$. $\bar{H}_r$ and $\bar{H}_z$ are the energies of the averaged Hamiltonians along z and r, respectively, at the s-resonance. The $s+1$ resonance then occurs at $\bar{H}_z + \delta\bar{H}_z$ and $\bar{H}_r + \delta\bar{H}_r$, where $\delta\bar{H}_r + \delta\bar{H}_z = 0$ to conserve total energy H.

$$\omega_z\left(\bar{H}_z + \delta\bar{H}_z\right) = (s+1)\frac{4}{3a}\left(F_r\bar{H}_r\right)^{1/4}\left(1 + \frac{\delta\bar{H}_r}{4\bar{H}_r}\right) \tag{56}$$

where we have used the expansion $\left(\bar{H}_r + \delta\bar{H}_r\right)^{1/4} \approx \bar{H}_r^{1/4}\left(1 + \delta\bar{H}_r/4\bar{H}_r\right)$. Expanding Eq. (56), and dropping the smallest term, we get:

$$\omega_z\left(\bar{H}_z + \delta\bar{H}_z\right) = s\frac{4}{3a}\left(F_r\bar{H}_r\right)^{1/4}\left(1 + \frac{\delta\bar{H}_r}{4\bar{H}_r}\right) + \frac{4}{3a}\left(F_r\bar{H}_r\right)^{1/4} \tag{57}$$

For $s < 10$ resonances, $s\left(\delta\bar{H}_r/4\bar{H}_r\right) \ll 1$. Thus Eq. (57) becomes:

$$\omega_z\left(\bar{H}_z + \delta\bar{H}_z\right) = s\frac{4}{3a}\left(F_r\bar{H}_r\right)^{1/4} + \frac{4}{3a}\left(F_r\bar{H}_r\right)^{1/4} \tag{58}$$

Combining Eq. (58) and (55) and using Eq. (44), we get an expression for $\delta\omega_z$

$$\delta\omega_z = |\omega_z\left(\bar{H}_z + \delta\bar{H}_z\right) - \omega_z\left(\bar{H}_z\right)| = \frac{4}{3a}\left(F_r\bar{H}_r\right)^{1/4} = \omega_r \tag{59}$$

Using $\triangle\omega_z = (\epsilon\alpha)^{1/2}\,\omega_z$ from Eq. (50), K_c becomes:

$$K_c = \frac{\triangle\omega_z}{\delta\omega_z} = (\epsilon\alpha)^{1/2}\,\frac{\omega_z}{\omega_r} \tag{60}$$

Thus the criterion for the overlapping of $q = 1$ resonances is:

$$K_c = (\epsilon\alpha)^{1/2}\,s > 1 \tag{61}$$

This actually sets the upper limit on K_c, since other resonances will overlap before the overlap of the $q = 1$ resonances, resulting in an onset of strong chaos at a lower value of K_c then that given by Eq. (61). The exact form of the dependence of ϵ and α on P and β is difficult to obtain, since it would require the expression of the full Hamiltonian given by Eq. (7) in action-angle variables. However, we can find the qualitative relationship between the two sets of variables and thereby explain the overlapping of resonances and the onset of strong chaos observed with variation of P or β. Multiplying out the terms in Eq. (7), we get:

$$V = \frac{1}{2}\left[\frac{P^2}{r^2} - P\left(1 - r^2 - \beta^2 z^2\right) + r^2\left(1 - r^2 - \beta^2 z^2\right)^2\right] \tag{62}$$

In $\triangle r$ coordinates (see Eq. (30), where the expansion around r_0 leads to the cancellation of linear terms), the second term in the above equation is quadratic, and the leading contribution from the first term is also quadratic, and therefore linear in the equations of motion. It follows that most of the nonlinearities in the Hamiltonian come from the third P-independent term, which also contains coupling. It can therefore be concluded that decreasing P will increase the relative contribution from the nonlinear and coupling terms, and therefore increase both the nonlinearity parameter α and the coupling ϵ. From Eq. (61), an increase in α, ϵ will result in a greater overlap of resonances and an eventual onset of strong chaos. Figure 8 shows a set of resonances well bounded by KAM curves, we therefore expect that $K_c \ll 1$ for this set of parameters. Figure 7, plotted for a lower value of P, shows an overlap of resonances. Although some of the island structure is retained and we can still see the location of the different s-resonances, the distruction of the bounding KAM curves has occured, resulting in greater region of stochasticity, as compared to Figure 8. Thus $K_c > 1$ in Figure 7, showing a transition to strong chaos.

An increase in β increases the overlap between resonances and therefore chaotic behavior by increasing ϵ in Eq. (61). This can be seen by looking at Eq. (10), where the coupling term is the last term in the equation. Since this term is strongly dependent on β, we can

expect that an increase in β will also increase the perturbation coefficient ϵ. The overlap of resonances and the onset of strong chaos caused by increasing β can be seen in Figs. 7, 9-11 where the value of β is varied, while P is kept constant.

Thus variation of P or β effects the degree of stochasticity through α and ϵ, which as shown in Eq. (61), determine the Chirikov parameter K_c.

III.E Adiabatic limit

Eq. (46) shows a linear dependence of s on β and a much weaker $-1/4$ power dependence on $\bar{H}_r$. As mentioned before, in the $z = 0$ subplane, the coordinates separate so that $\bar{H}_r$ and $\bar{H}_z$ can be replaced by H_r and H_z, respectively (see Eq. 45), as long as the motion is not too affected by the resonance. Using Eq. (46), we expect a decrease in β to strongly shift the location of a one-to-one resonance towards smaller values of H_r or closer to the midpoint of oscillation at $r = r_h$, in the $z = 0$ plane. Figure 11 shows this for $\beta = 1/2$. There is only a thin layer of stochasticity close to the separatrix, due to the very low values of H_r (or amplitude of oscillation A) where the resonance occurs.

As the value of β is further decreased, the quadratic terms in Eq. (28) can no longer be neglected, leading to behavior different than what would be expected based on previous analysis (Figures 12 and 13). To understand the motion at $\beta^2 \ll 1$, let us turn to Eqs. (10) and (11). It can be seen that there is a separation of time scales between r and z motion in the limit of small β. Since the motion along r is much faster than the motion along z, J_r is a conserved adiabatic invariant, except during the crossing of the separatrix [17, 19, 20]. At the approach to the separatrix the frequency, ω_r, slows down leading to a break-down of $\omega_r \gg \omega_z$ condition required for the adiabatic invariance of J_r. The change in J_r during each crossing is $\sim \beta ln\,(\beta)$. [21] This leads to mostly chaotic orbits inside and close to the separatrix as shown in Figure 13.

To avoid the crossing of the separatrix that occurs during a transition between cyclotron and figure-8 orbits, the action J_r has to be high enough so that the ion executes a figure-8 orbit with $\omega_r \gg \omega_z$ when it passes $z = 0$ subplane. To ensure the adiabatic invariance of J_r, we can find a lower limit on its value by choosing $H_{rmin} = (1 + \delta_c)\, V\,(r_h, 0)$, where $\delta_c \ll 1$ [22], calculating the resultant p_r as a function of r, and substituting it into the integral in

Eq. (15). The condition for integrable orbits becomes:

$$J_r > \frac{1}{2\pi} \oint \left\{ (1+\delta_c)\, V\left(r_h, 0\right) - \left[\frac{P}{r} - r\left(1 - r^2\right) \right]^2 \right\}^{\frac{1}{2}} dr \tag{63}$$

The above integral is the action of the ion in the $z = 0$ subspace when H_r is just high enough for the ion to pass over the energy barrier at some finite speed and execute figure-8 orbits. $r_h^2 = K_1$ is the location of the top of the barrier evaluated at $z = 0$ (Equation 26). The factor of $(1 + \delta_c)$ insures that the motion is not too close to the phase-space separatrix. Since J_r is conserved for integrable orbits, Eq. (63) provides a threshold above which orbits are integrable.

Figure 14 shows the area inside the phase space separatrix, J_{rs}, in the $z = 0$ cross-section as a function of P. All orbits passing through the $z = 0$ plane with $J < J_{rs}$, will cross the separatrix as the area inside shrinks with motion towards higher $|z|$ values. This leads to mostly chaotic orbits inside and close to the separatrix as shown in Figure 13. The shrinking of the area inside the phase-space separatrix is due to the drop of the potential barrier along r as the ion moves towards higher absolute values of z (see Figure 3). Thus most of the cyclotron orbits in the low β limit should be stochastic due to a repeated violation of J_r. Above a critical value of $P = P_c$, all cyclotron orbits disappear and only betatron orbits exist, we would therefore expect mostly integrable orbits.

UNIVERSAL RESONANCE AND INTRINSIC DEGENERACY

At higher values of P, the quadratic terms become more important for ions confined to the FRC. This can be seen in Figure 5 where the quadratic coefficient crosses zero below P_c (if the amplitude terms are taken into account) and continues to increase as P increases. It follows that at higher values of P (about $P > 6P_c/5$ for the energies used), the unperturbed Hamiltonian can be expressed as uncoupled simple harmonic oscillators. Expanding the Hamiltonian in Eq. (7) around $r_0 = K_1^{1/2}$, so that $\triangle r = r - r_0$, and grouping all non-quadratic terms under the perturbation term, H_1, we get

$$H = \frac{1}{2}p_r^2 + \frac{1}{2}p_z^2 + \frac{1}{2}D_{r0}\triangle r^2 + \frac{1}{2}\beta^2 D_{z0} z^2 + \epsilon H_1\left(r, z\right) \tag{64}$$

where D_{r0} and $\beta^2 D_{z0}$ are the coefficients of the quadratic coordinate terms in the expansion of the Hamiltonian

$$D_{r0} = 1 + 2P - 12K_1 + 15K_1^2 + \frac{3P^2}{K_1^2} \tag{65}$$

$$\beta^2 D_{z0} = \beta^2 \left(2P - 2K_1 + 2K_1^2\right) \tag{66}$$

with K_1 is given by Eq. (27).

In action-angle variables the coordinates of a simple harmonic oscillator are given by [7]

$$\triangle r = \left(\frac{2J_r}{R_r}\right)^{1/2} sin\theta_r \tag{67}$$

$$p_r = (2J_r R_r)^{1/2} cos\theta_r \tag{68}$$

$$z = \left(\frac{2J_z}{R_z}\right)^{1/2} sin\theta_z \tag{69}$$

$$p_z = (2J_z R_z)^{1/2} cos\theta_z \tag{70}$$

where $R_r = D_{r0}^{1/2}$ and $R_z = \beta D_{z0}^{1/2}$. Substituting action-angle variables from Eq. (67), (68), (69), and (70) into the expanded Hamiltonian in Eq. (64), we get

$$H = \omega_r J_r + \omega_z J_z + \epsilon H_1 \left(\vec{J}, \vec{\theta}\right) \tag{71}$$

where ω_r and ω_z are the frequencies of the unperturbed quadratic Hamiltonian,

$$\omega_r = D_{r0}^{1/2} \qquad \omega_z = \beta D_{z0}^{1/2} \tag{72}$$

In action-angle variables, H_1 can be expanded as:

$$H_1 = \sum_{l,m=-\infty}^{\infty} H_{l,m}\left(\vec{J}\right) exp\left(i\vec{n}\cdot\vec{\theta}\right) \tag{73}$$

In the absence of resonances, Eq. (71) is integrable and the conserved invariants, close to J_r and J_z, can be found by applying standard perturbation theory and expanding in the same way as for a one-dimensional system. The terms in H_1 can be easily found by expanding the Hamiltonian around r_0, as was done in Eq. (64), and substituting action-angle variables, given by Eqs. (67)-(70). The exact expression for $H_{1,-1}$ will be given below, relating to a discussion of a $1:1$ universal resonance.

A resonance will occur whenever the conditions of Eq. (24) are satisfied, with ω_r and ω_z given by Eq. (72). The width of the island in a resonance for a Hamiltonian given by Eq.

(71) should be large, due to the intrinsic degeneracy, since the unperturbed frequencies, ω_r and ω_z, are constant, thereby leading to a universal resonance. In this case, transforming to a rotating frame:

$$J_r = s\hat{J}_1; \qquad J_z = \hat{J}_2 - q\hat{J}_1; \qquad \hat{\theta}_1 = s\theta_r - q\theta_z; \qquad \hat{\theta}_2 = \theta_z \tag{74}$$

the unperturbed Hamiltonian in Eq. (71) is a function of $qJ_r + sJ_z$ (where $\omega_z/\omega_r = s/q$) or in rotating coordinates:

$$\hat{H}_0 = \hat{H}_0\left(\hat{J}_2\right) \tag{75}$$

that is, H_0 is independent of $\hat{J}_1$.

Following Lichtenberg and Lieberman [7], in the presence of a resonance in an intrinsically degenerate system (where ω_r and ω_z are constant), the perturbation to the Hamiltonian is

$$\triangle\bar{H} = \frac{1}{2}G\left(\triangle\hat{J}_1\right)^2 + \frac{1}{2}F\left(\triangle\hat{\theta}_1\right)^2 \tag{76}$$

where the bar above $\triangle H$ signifies that averaging over the fast variable $\hat{\theta}_2$ has been performed. G is a nonlinearity parameter proportional to ϵ

$$G = \epsilon\frac{\partial^2 H_{0,0}}{\partial\hat{J}_{10}^2} + \epsilon\frac{\partial^2 H_{s,-q}}{\partial\hat{J}_{10}^2} \tag{77}$$

F is also proportional to ϵ,

$$F = -2\epsilon H_{s,-q} \tag{78}$$

Eq. (76) was obtained by transforming to rotating coordinates $\vec{\hat{J}}$ and $\vec{\hat{\theta}}$, where $\hat{\theta}_1$ and $\hat{\theta}_2$ are the slow and fast variables, respectively. Then averaging over the fast variable $\hat{\theta}_2$, and expanding the highest order resonant terms around the elliptic point of the resonance at $\hat{J}_1 = \hat{J}_{10}$ and $\hat{\theta}_1 = 0$. Since the nonlinearity parameter G in Eq. (76) is small (of order ϵ), we can expect maximum excursion in $\triangle\hat{J}_1$ to be large. This explains why intrinsically degenerate systems have large resonances [7].

The equations given above can be used for analytic study of specific resonances that occur at different values of β. Equations (65) and (66) determine the range of values of P and β for which different resonances occur. Figure 15 shows D_{r0} and $\beta^2 D_{z0}$ for $\beta = 2$ plotted as a function of P. It can be seen that the two coefficients are close for a range of values of P, creating a universal one-to-one resonance. To estimate $\triangle\bar{H}$ and $\triangle\hat{J}_1$, (or $\triangle J_r$), for the case of the one-to-one resonance, we express ϵH_1 in action-angle variables and find G and

$F = -2\epsilon H_{1,-1}$, in accordance with Eqs. (77) and (78). Changing back to (J_r, J_z) variables, keeping only the terms of lowest power in $\vec{J}$, a valid approximation for ions confined inside the FRC, we get

$$G \approx \frac{1}{R_r^2}\left(6K_1 + \frac{15P^2}{2K_1^3}\right) \tag{79}$$

$$F \approx \frac{1}{2R_r^2}\left(6K_1 - 1\right) J_r J_z \tag{80}$$

To compare the magnitudes of G and F, keep in mind that $K_1^{1/2}$ is the midpoint of oscillation in the $z = 0$ subplane, so that for the ions oscillating inside the FRC: $K_1 \sim 1/2$. In dimensionless variables adopted throughout this paper, the magnetic field separatrix (to be distinguished from the phase-space separatrix) at $z = 0$ is located at $r = 1$. From Eq. 76 the maximum fluctuation in energy for a one-to-one resonance is given by,

$$\triangle \bar{H} \approx \left(\pi^2/2\right) F \tag{81}$$

with F given by Eq. (80). The maximum change in J_r for a one-to-one resonance can be estimated by setting $J_r = \hat{J}_1$ (see Eq. (74)) and using Eq. (76) to obtain:

$$\left(\frac{G}{F}\right)^{1/2}\left(\frac{\triangle J_{rmax}}{\pi}\right) = O(1) \tag{82}$$

Substituting Eqs. (79) and (80) into Eq. (82), using $J_r \sim J_z$, we get,

$$\frac{\triangle J_{rmax}}{J_r} \sim O\left(1\right) \tag{83}$$

indicating that the changes in action in a universal resonance are large. Figure 16 shows a universal one-to-one resonance that occurs at $\beta = 2$ for a range of values of P. The fluctuations caused by the resonace are large due to the intrinsic degeneracy of the system in this regime.

CONCLUSION

After reducing the three-dimensional Hamiltonian of an ion inside the FRC to that of a particle moving in a two-dimensional potential, possible types of ion orbits for positive azimuthal angular momentum P were derived. Then the effects of variation in P and inverse elongation β were investigated. A method of averaging was used to study the structure of nonlinear resonances. It turns out that at intermediate values of P, the fourth order terms in

the averaged Hamiltonian predominate. In this case, the unperturbed frequencies ω_r and ω_z can be derived as a function of the averaged Hamiltonians $\hat{H}_r$ and $\hat{H}_z$, respectively. Based on these frequencies, the occurance of various s resonances, where $s = \omega_z/\omega_r$, can be calculated. It was found that increasing β shifts the location of the resonance outward towards higher values of $\hat{H}_r$. High values of β are found to produce high s resonances. The structure of the resonances was such that higher s resonances were found closer to the midpoint of oscillation along r. The dependence of Chirikov's island overlap parameter, K_c, on the magnitude of the perturbation ϵ and nonlinearity α was derived and the qualitative relationship between ϵ, α and β, P discussed. It was found that lowering P or increasing β cause an increase in ϵ and α, leading to a greater overlap of resonances and the eventual onset of strong chaos. In the adiabatic regime, occuring for large elongations (small β), orbits outside the phase-space separatrix, in the $z = 0$ subplane were shown to be integrable, while the majority of orbits inside the phase-space separatrix were not. This is due to separation of time scales $\omega_r \gg \omega_z$ that occurs for orbits which do not cross the phase-space separatrix.

Next, the universal resonance resulting from intrinsic degeneracy of the Hamiltonian at higher values of P was investigated. Under these circumstances, the unperturbed frequencies are constant, and the Hamiltonian can be expressed in action-angle variables of a simple harmonic oscillator. The width of the resonances can then be derived from the perturbation term H_1. For high P case, most of the orbits are integrable, except in case of a resonance when $\omega_z/\omega_r = q/s$, where q and s are integers. After deriving an expression for unperturbed frequencies in this degenerate regime, a universal one-to-one resonance was found analytically and numerically at $\beta = 2$ for a range of values of P. The width of this resonance was estimated and the fluctuations in action found to be large (of order one), as would be expected for a degenerate case.

Acknowledgements: This work was supported, in part, by U.S. Department of Energy Contract No. DE-FG02-92ER54184

References

* Electronic address: <landsman@princeton.edu>

[1] M. Tuszewski, Review Paper: Field Reversed Configurations. Nucl. Fusion **28**, 2033-92 (1988).

[2] M. Tuszewski, D. P. Taggart, R. Chrien, D. J. Rej, R. E. Siemon, and B. L. Wright, Axial dynamics in field-reversed theta pinches. Phys. Fluids **B3**, 2856-70 (1991).

[3] J. P. Friedberg and S. W. Haney, Variational methods for studying tokamak stability in the presence of a thin resistive wall. Physics of Fluids **B1**, 1637-45 (1989).

[4] J. M. Finn and R. N. Sudan, Review Paper: Field Reversed Configurations with a component of energetic particles. Nucl. Fusion **22**, 1443-1518 (1982).

[5] A. H. Glasser and S. A. Cohen, Ion and electron acceleration in the field-reversed configuration with odd-parity rotating magnetic field. Phys. Plasmas **9**, 2093-2102 (2002).

[6] R. Z. Sagdeev D. A. Usikov and G. M. Zaslavsky, *Nonlinear Physics* (Harwood Academic Publishers, Philadelphia, 1992).

[7] A. J. Lichtenberg and M. A. Lieberman, *Regular and Chaotic Dynamics* (Springer-Verlag, New York, 1992).

[8] G. M. Zaslavsky, *Physics of chaos in Hamiltonian systems* (Imperial College Press, London, 1998).

[9] A.C. J. Luo and R.P. S. Han, Analytical predictions of chaos in a non-linear rod. J. Sound and Vibration **227(3)**, 523-44 (1999).

[10] A.C. J. Luo and R.P. S. Han, The dynamics of stochastic and resonant layers in a periodically driven pendulum. Chaos, Solitons and Fractals **11**, 2349-59 (1999).

[11] G. M. Zaslavsky and N. N. Filonenko, Stochastic instability of trapped particles and conditions of application of the quasi-linear approximation. Sov. Phys. JETP **27**, 251-57 (1968).

[12] A.C. J. Luo, Resonant layers in a parametrically excited pendulum. Int. J. Bifurcations and Chaos **12(2)**, 409-19 (2002).

[13] H. Goldstein, *Classical Mechanics* (Addison-Wesley, Reading, 1980).

[14] L. S. Solov'ev, The theory of hydromagnetic stability of toroidal plasma configurations. Sov. Phys. JETP **26**, 400-7 (1968).

[15] W. Hugrass and M. Turley, The orbits of electrons and ions in the fields of the rotamak. J.

Plasma Phys. **37**, 1-13 (1987).

[16] M. Y. Wang and G. H. Miley, Particle orbits in field-reversed mirrors. Nucl. Fusion **19**, 39-49 (1979).

[17] A. S. Landsman, S. A. Cohen and A. H. Glasser, Regular and stochastic orbits of ions in a highly prolate field-reversed configuration. To appear in Phys. Plasmas, (2004).

[18] S. A. Cohen and A. H. Glasser, Ion heating in the field-reversed configuration by rotating magnetic fields near the ion-cyclotron resonance. Phys. Rev. Letters **85**, 5114-5117 (2000).

[19] J.-S. Kim and J. R. Cary, Charged particle motion near a linear magnetic null. Phys. Fluids **26**, 2167 (1983).

[20] A. I. Neishtadt, Change of an adiabatic invariant at a separatrix. Sov. J. Plasma Phys. **12**, 568-573 (1986).

[21] J. R. Cary, D. F. Escande, and J. L. Tennyson, Adiabatic invariant changes due to separatrix crossing. Phys. Rev. A **34**, 4256-4275 (1986).

[22] A. I. Neishtadt, Stable periodic motions in the problem of passage through separatrix. Chaos **7**, 2-11 (1997).

List of Figures

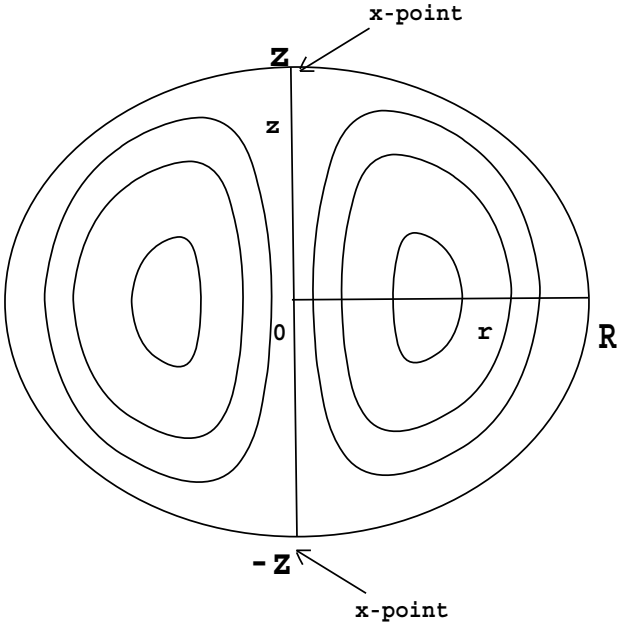

FIG. 1: Geometry of the Field-Reverse-Configuration of magnetic field. Lines correspond to the cross-section of surfaces of constant magnetic flux, Φ (See Eq. (2).

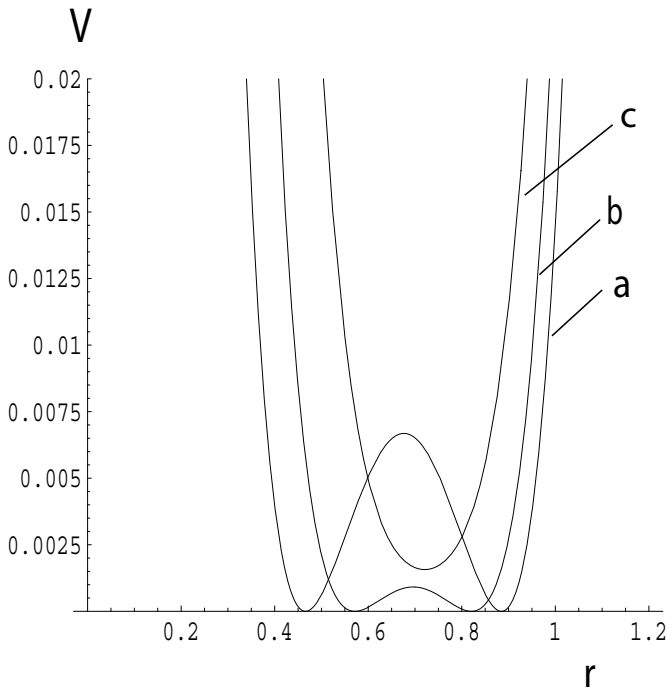

FIG. 2: Possible shapes of potential in the $z = 0$ subplane. a) P=.17 b) P=.22 c) P=.29 Below $P = P_c = 1/4$, the potential has a shape of a double well, and above a raised single well. The top of the potential barrier occurs at $r_h(P, z)$, see Eq. (26)

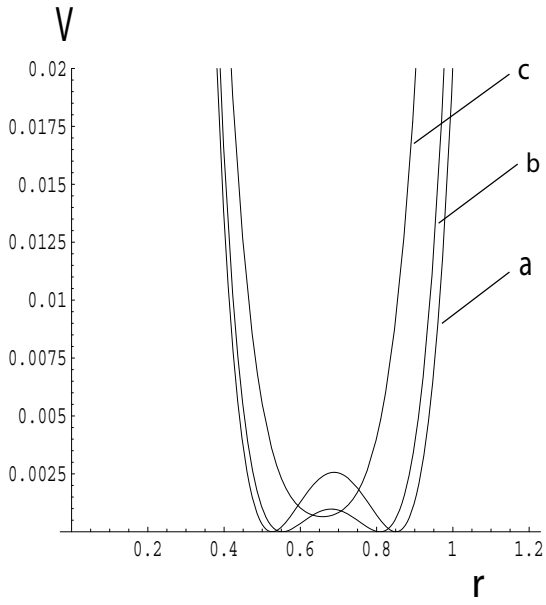

FIG. 3: Cross-sections of the potential V for $P = .2$: a) z=0; b) z=.2; c) z=.3 For positive P ions, the barrier in the double potential drops as $|z|$ increases, until it turns into a single raised potential. The barrier between the two zeros in the potential is the $\dot{\phi} < 0$ part of the orbit, while $\dot{\phi} > 0$ to the left and to the right of the potential barrier.

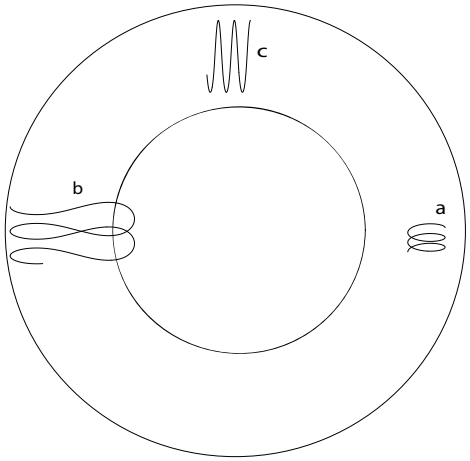

FIG. 4: Possible types of particle orbits for $P > 0$. Orbits are taken in the $z = 0$ invariant subspace. The outer circle indicates the zero in magnetic flux, Φ (also the boundary of the vessel). The inner circle is the location of the magnetic null, where field reversal occurs. a) Cyclotron orbit: ion oscillates in the outer portion of a double well, $P = .2$; b) Figure-8 orbit: ion oscillates over the entire double well, $P = .2$; c) Betatron orbits: oscillations in a raised potential, $P = .35$

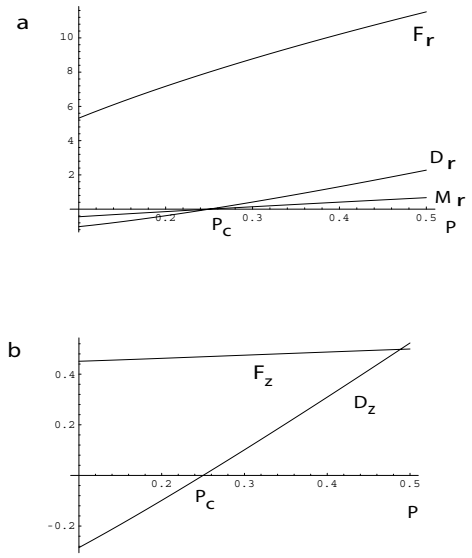

FIG. 5: Approximate coefficients for the averaged motion, neglecting amplitude contributions. a) F_r is the coefficient for the fourth power term of $\bar{H}_r$. D_r and M_r are coefficients for the quadratic and third power terms, respectively. Although they seem to intersect the x-axis around $P \approx P_c$, amplitude dependent terms cause D_r and M_r to shift upwards, lowering the value of P at which these terms are negligible. b) F_z is the coefficient for the fourth power term of $\bar{H}_z$ and D_z is the coefficient for the quadratic term. Like in the above case, higher order amplitude dependent terms cause D_z to shift upwards.

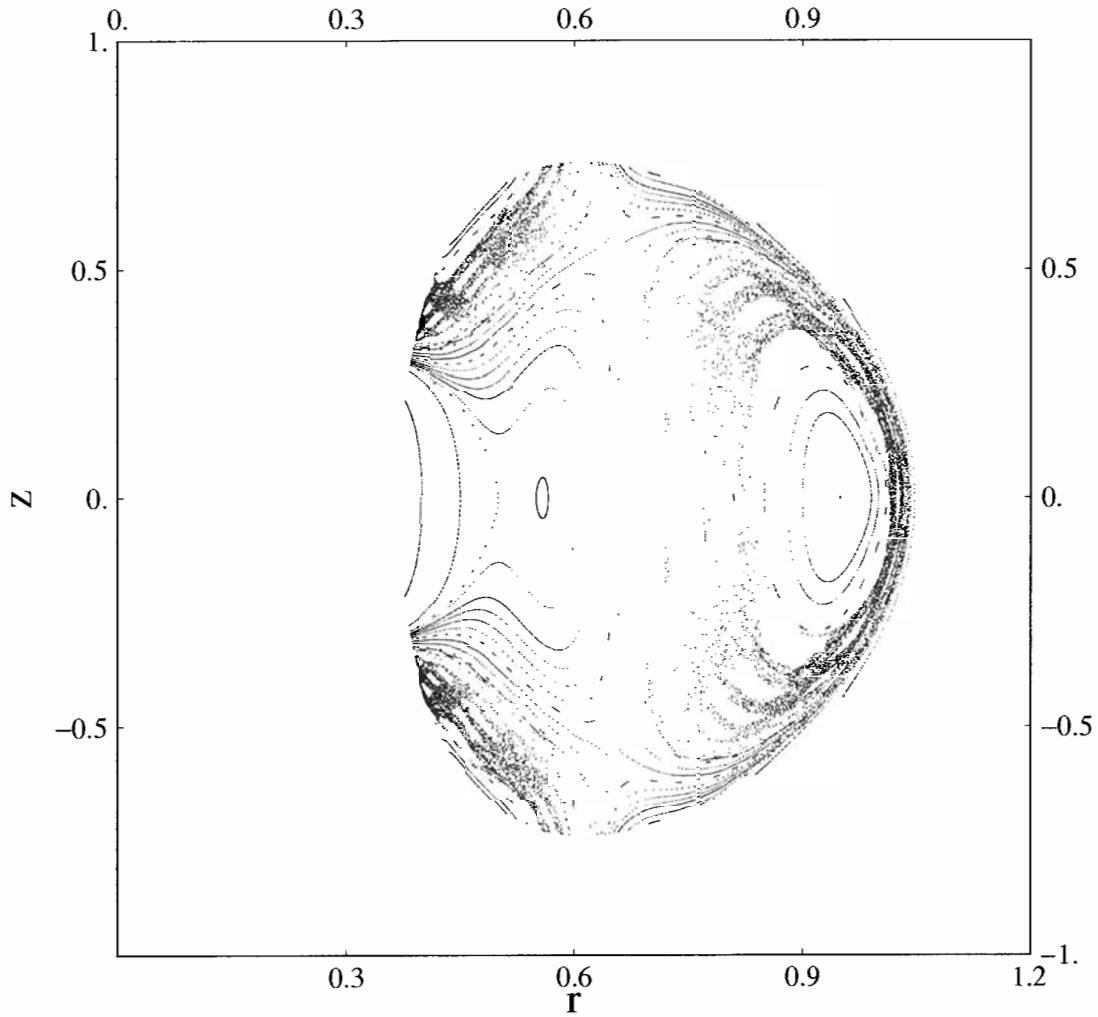

FIG. 6: Cross-section of a trajectory inside the FRC exploring most of the vessel while remaining within its boundaries. Boundary of the vessel occurs at $\Phi = \left(1 - r^2 - \beta^2 z^2\right) = 0$. Plotted in scaled dimensionless variables, E denotes total energy. $E = .063$, $\dot{r} = 0$, $P = .25$, $\beta = 1$

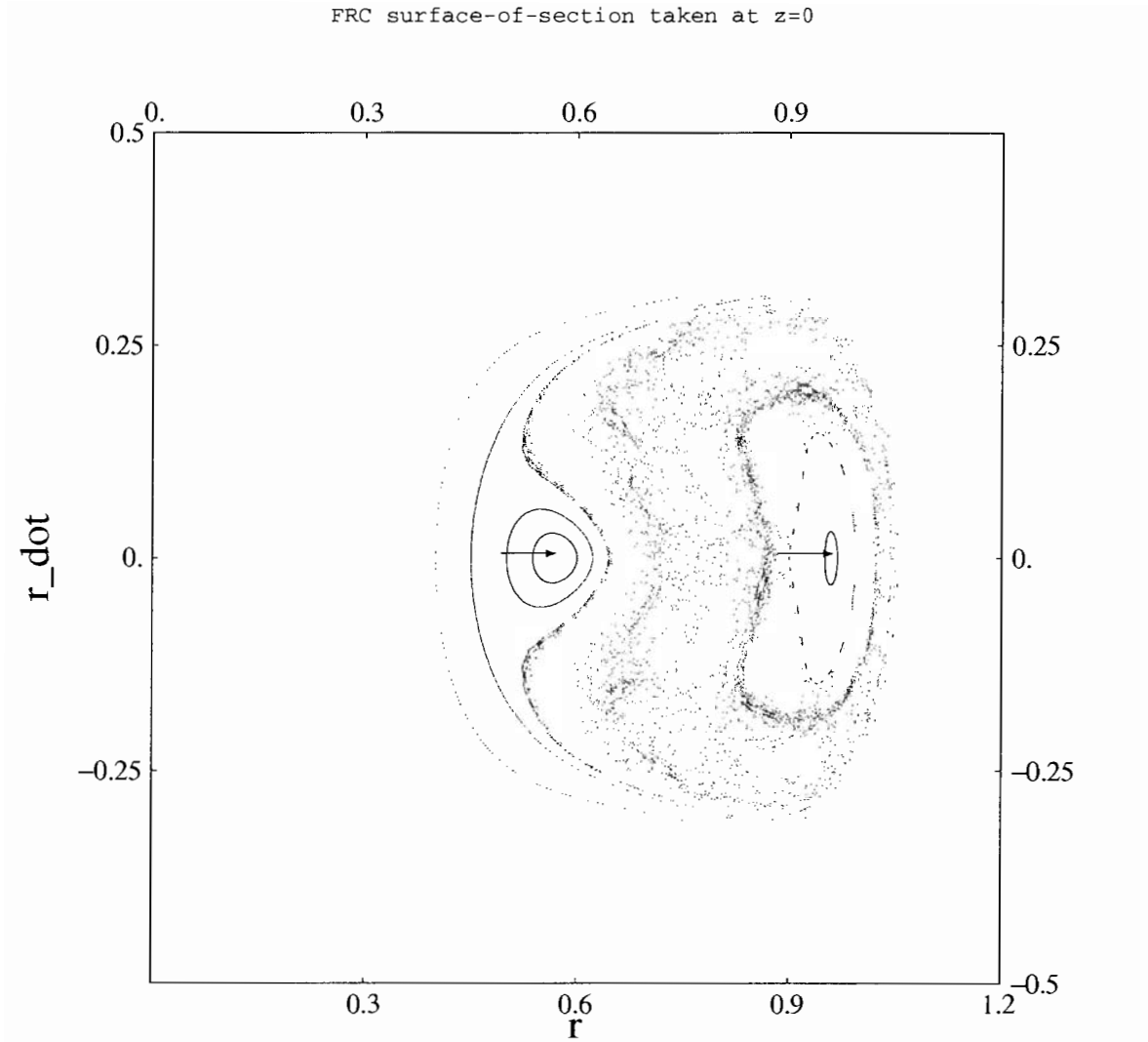

FIG. 7: Overlapping of resonances, leading to an onset of strong chaos (compare with Figure (8)). The arrows in the figure point to the elliptic centers of the $1:1$ resonances. The number of islands increases near the midpoint, $r_h \approx .7$. $E = .063$, $P = .23$, $\beta = 1$

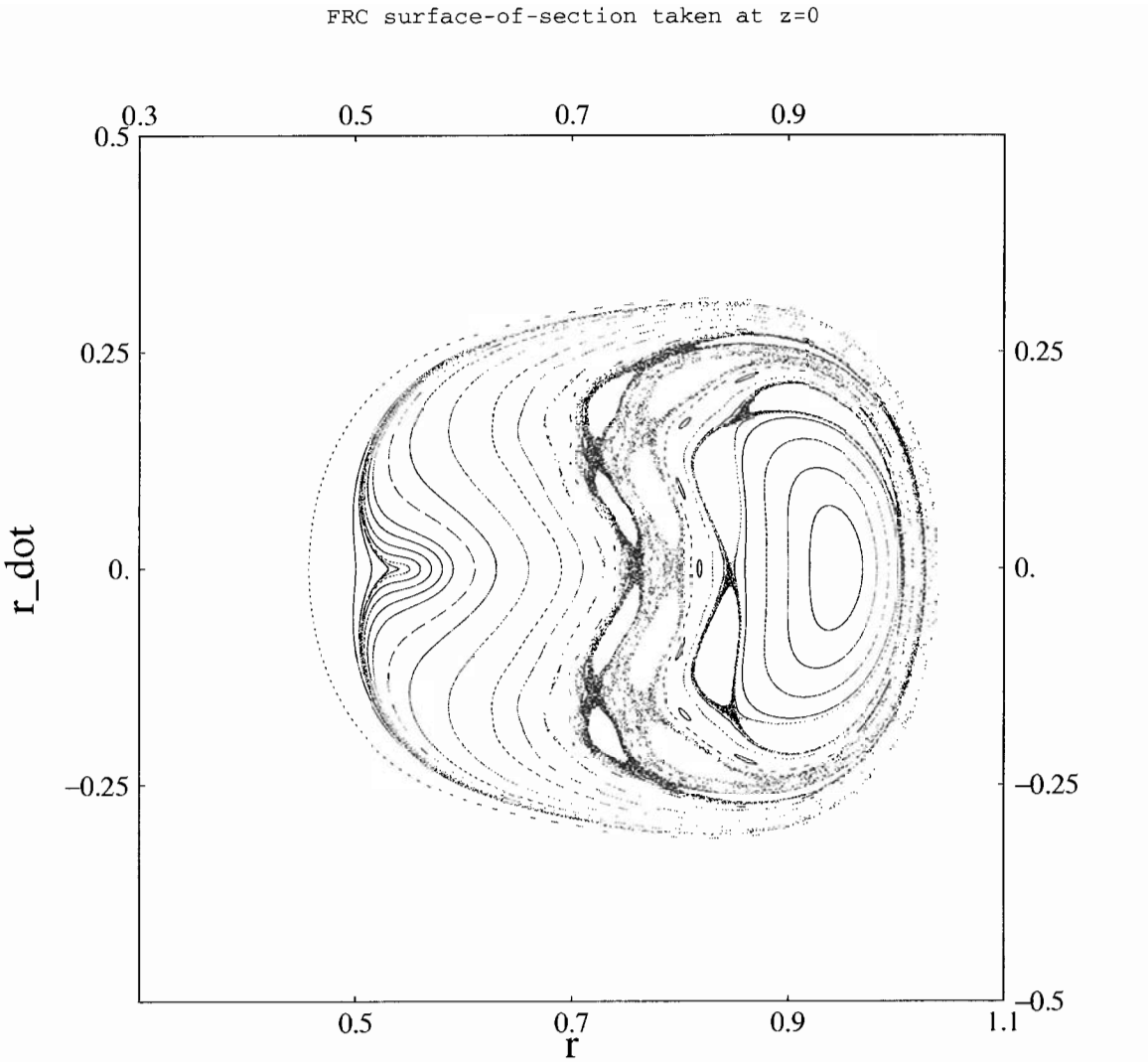

FIG. 8: Set of nonlinear resonances separated by KAM curves. The number of islands increases closer to the midpoint of oscillation, r_h, where $r_h \approx .7$. $E = .063$, $P = .258$, $\beta = 1$

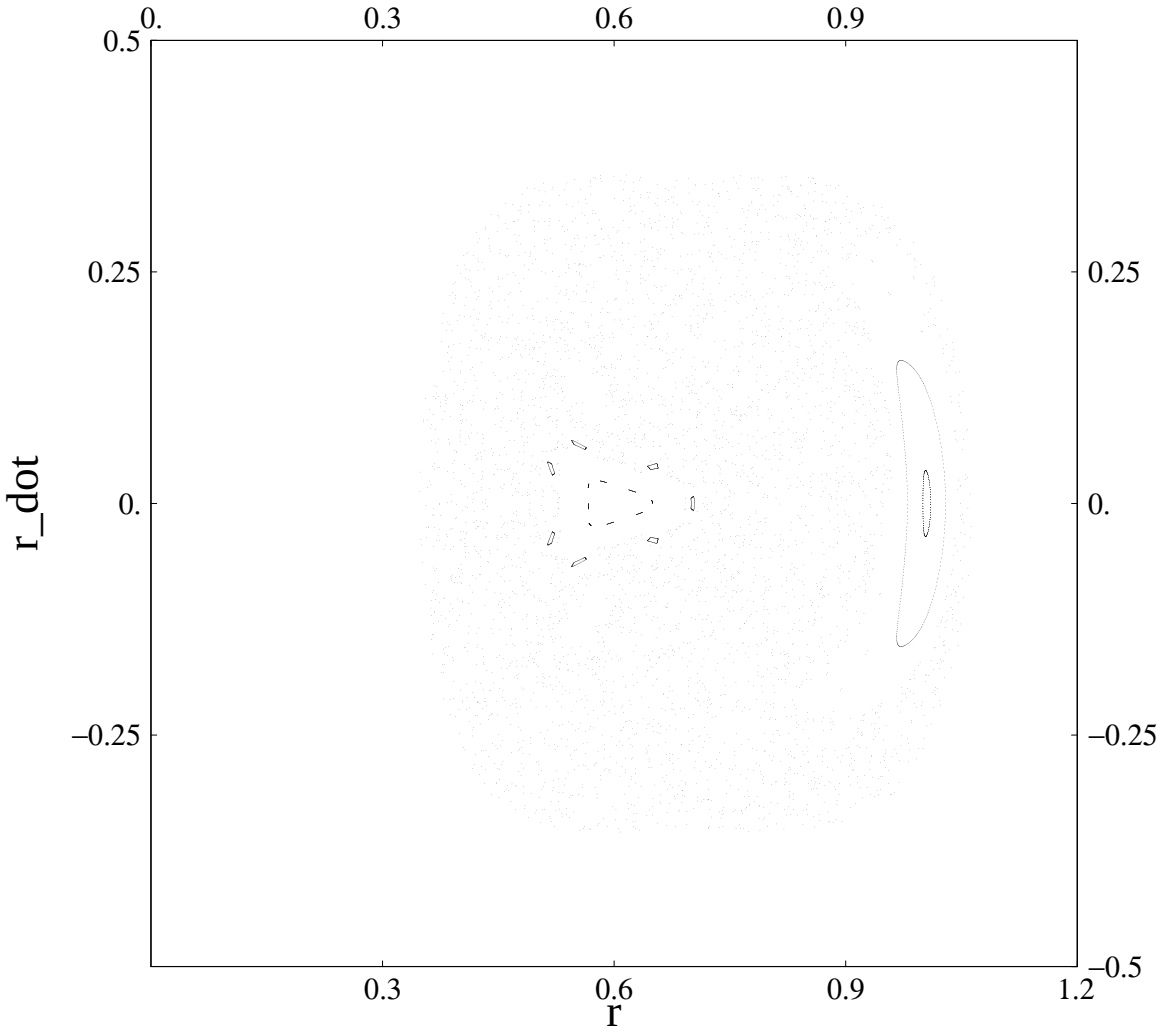

FIG. 9: Outward shift of the outer 1 : 1 resonance due to an increase in β in a strongly chaotic regime (compare with Figure (7)). $E = .063$, $P = .23$, $\beta = 1.2$

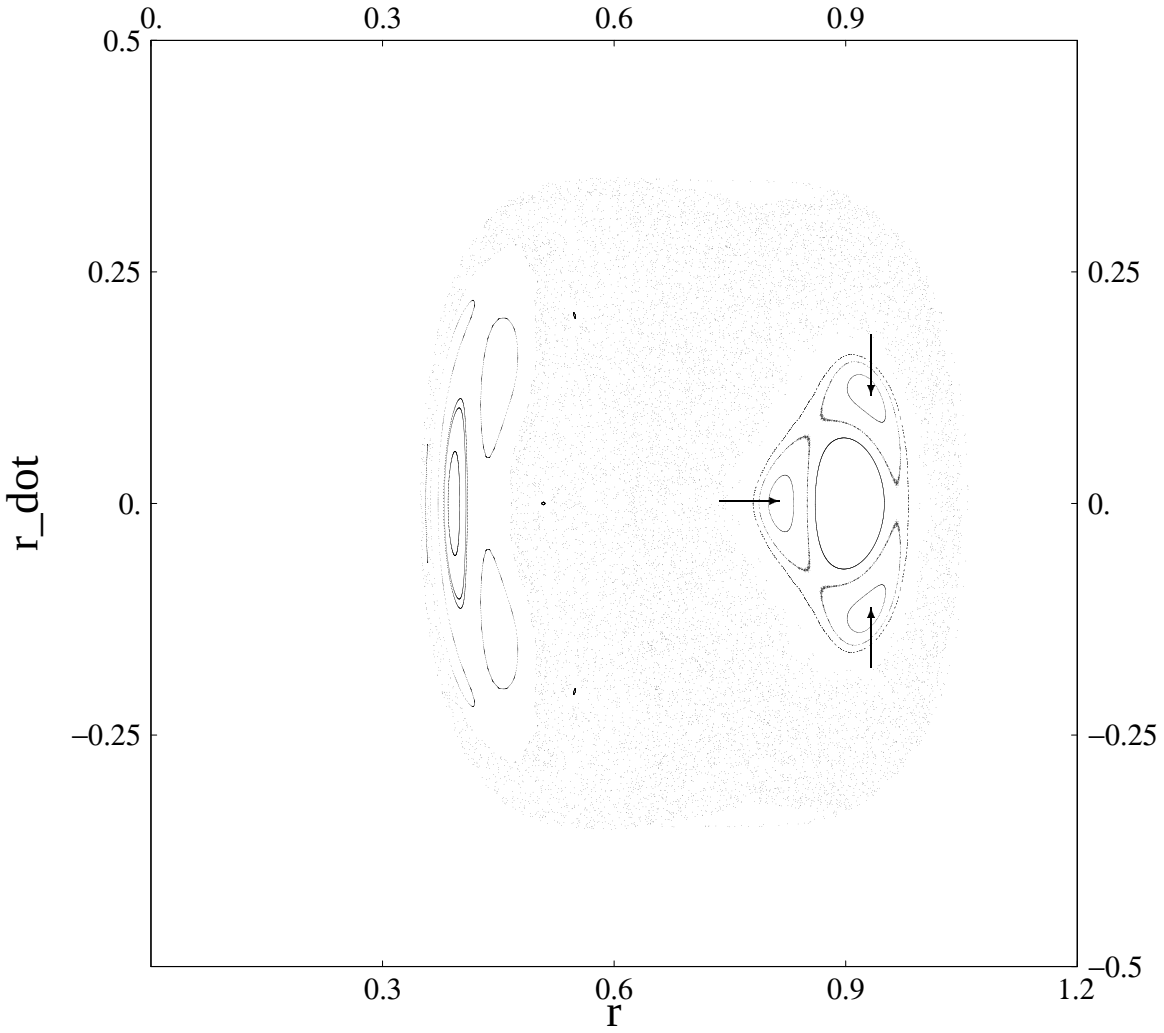

FIG. 10: Resonance at higher β. Arrows point to the elliptic centers of the outer 3 : 2 resonance. $E = .063$, $P = .23$, $\beta = 2$

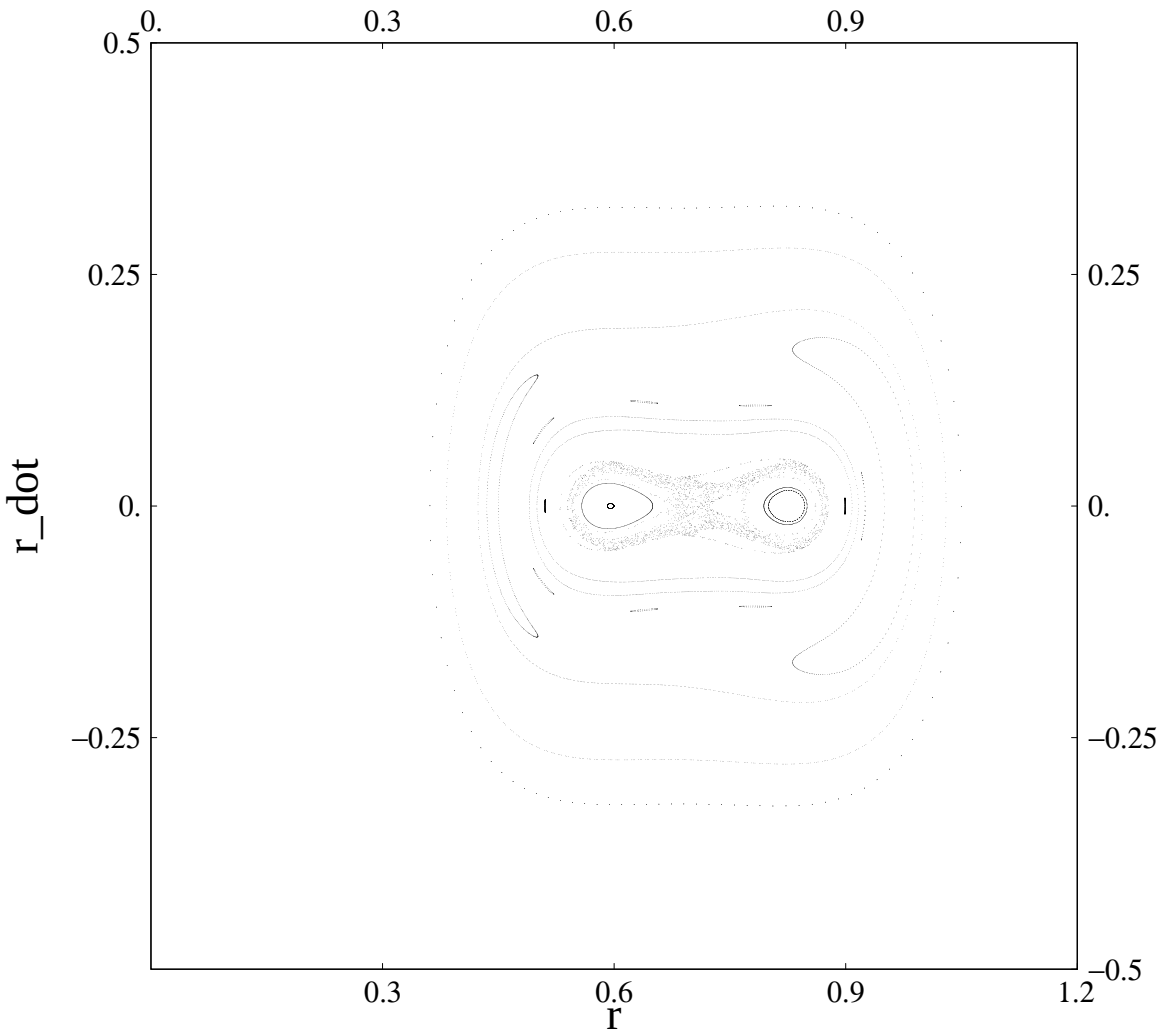

FIG. 11: Shifting of resonances towards the midpoint and the decrease of chaos with decreasing β. Location of $1:1$ resonances shifts closer to the midpoint of oscillation, $r_h \approx .7$, as β is lowered. $E = .063$, $P = .23$, $\beta = 1/2$

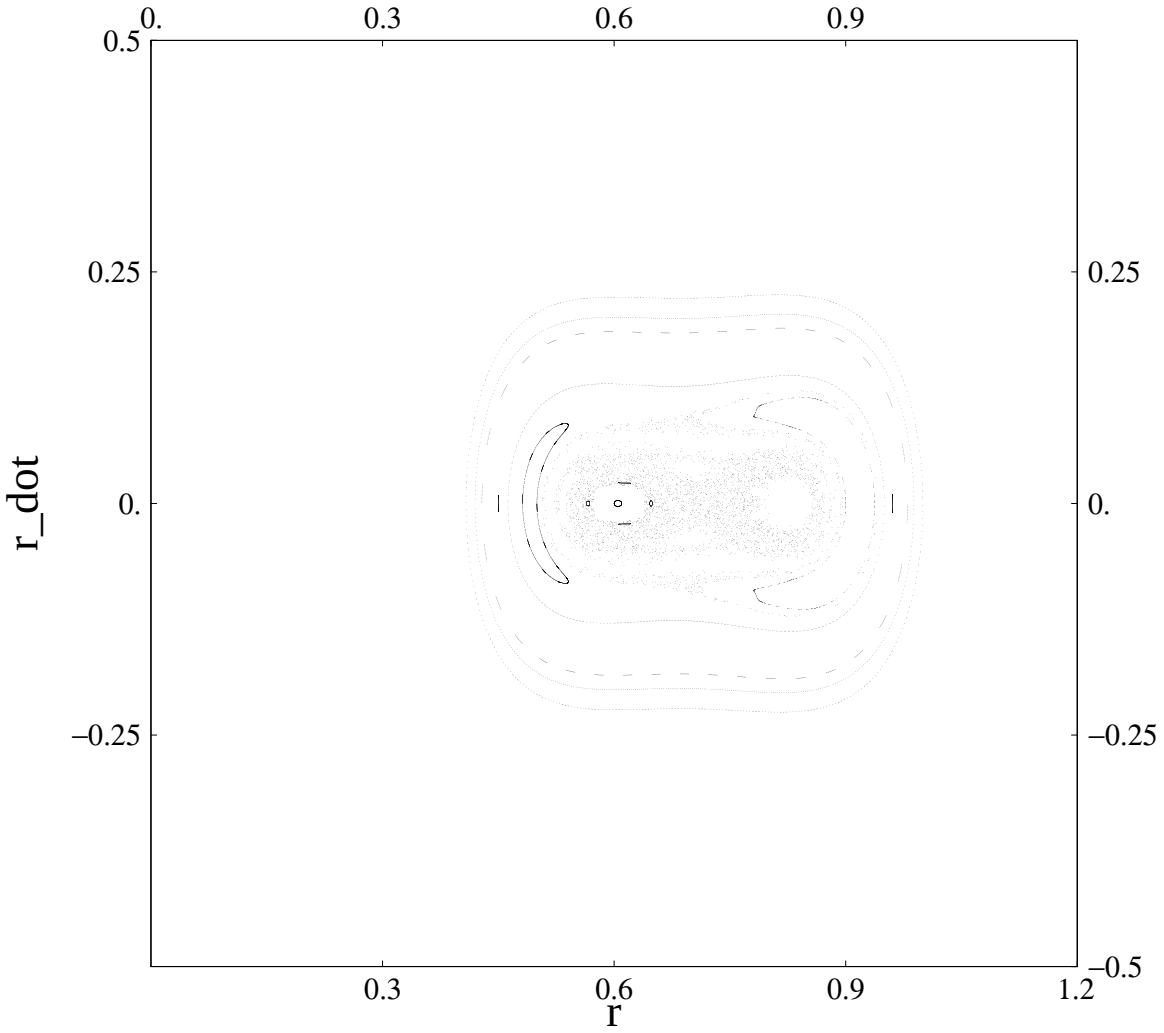

FIG. 12: Chaos at lower values of β where the quartic approximation fails. $E = .063$, $P = .23$, $\beta = .3$

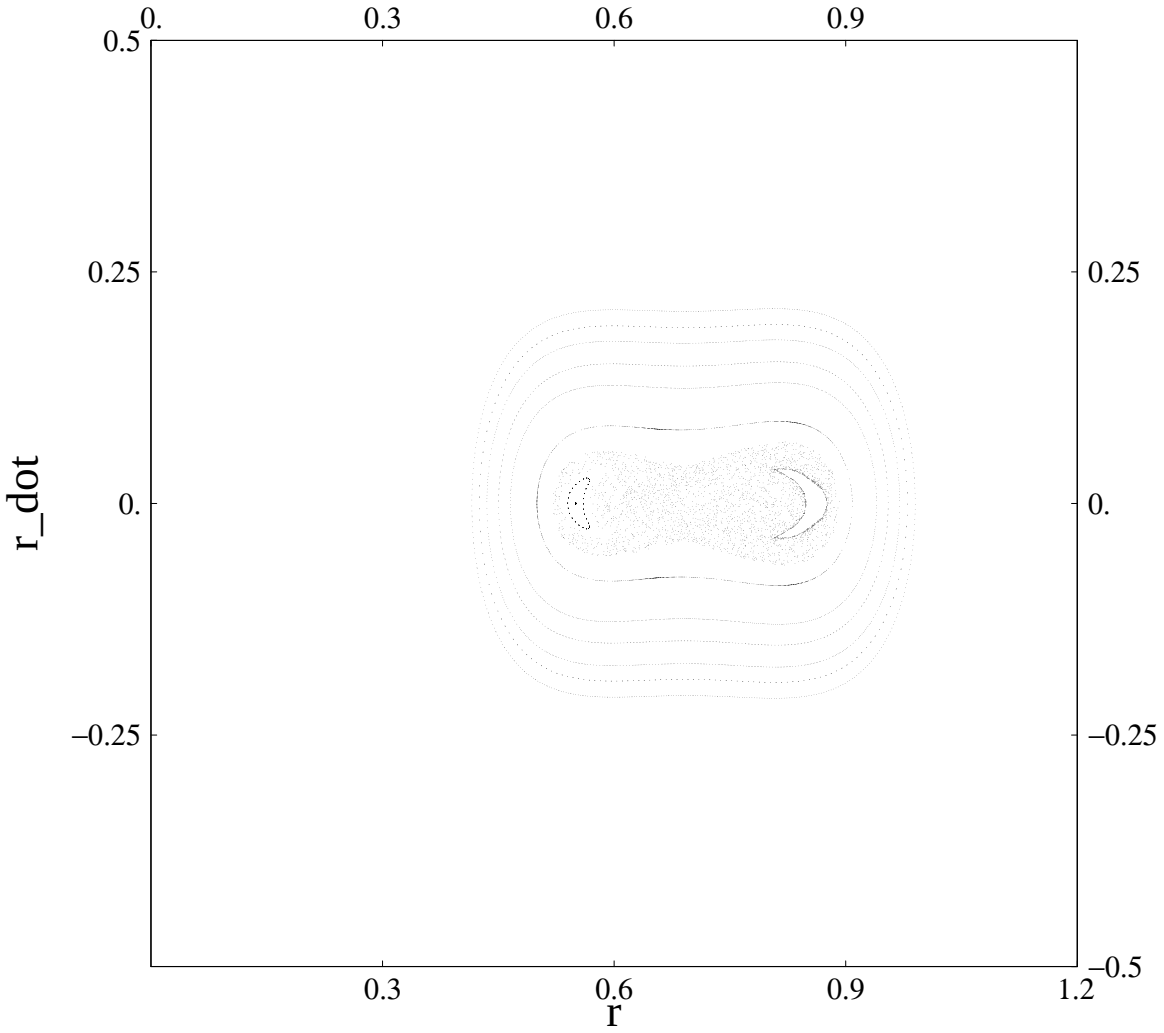

FIG. 13: The adiabatic limit occuring for small β values. Most orbits inside and close to the separatrix are chaotic. $E = .063$, $P = .23$, $\beta = .2$

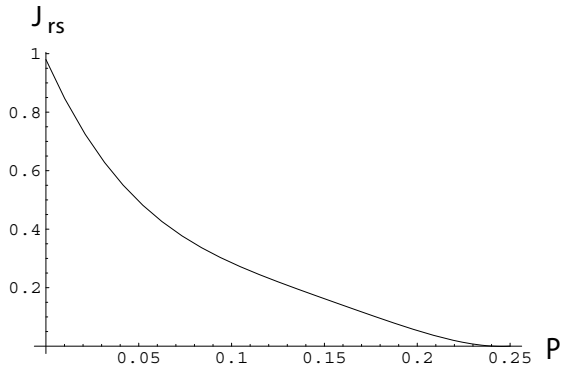

FIG. 14: The area inside the phase-space separatrix, J_{rs}, in the $z = 0$ cross-section as a function of P.

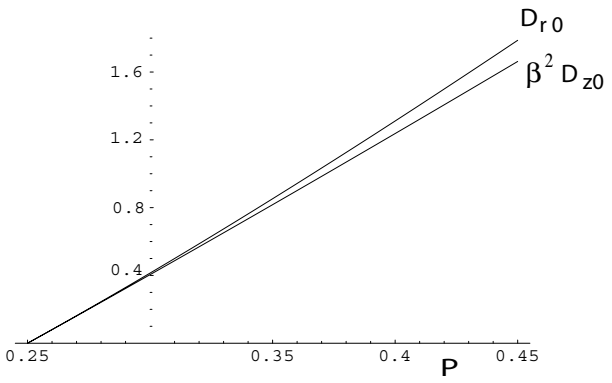

FIG. 15: Quadratic coefficients of H_0 as a function of P for the case of a universal $1:1$ resonance at $\beta = 2$. Below $P = .25$ fourth power terms dominate.

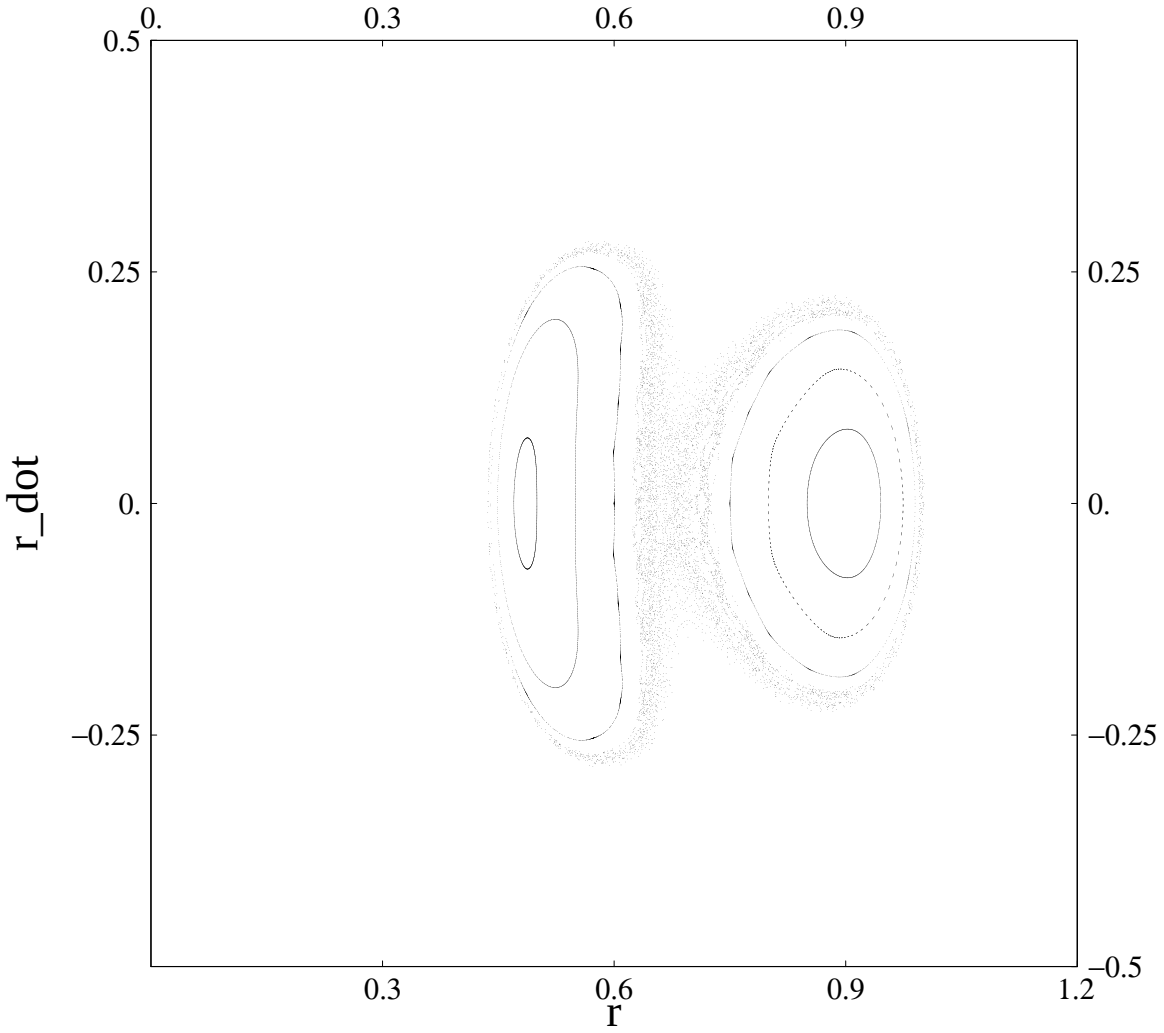

FIG. 16: Universal $1:1$ resonance occuring as a result of intrinsic degeneracy, onset at higher P values. $E = .063$, $P = .3$, $\beta = 2$

External Distribution

Plasma Research Laboratory, Australian National University, Australia

Professor I.R. Jones, Flinders University, Australia

Professor João Canalle, Instituto de Fisica DEQ/IF - UERJ, Brazil

Mr. Gerson O. Ludwig, Instituto Nacional de Pesquisas, Brazil

Dr. P.H. Sakanaka, Instituto Fisica, Brazil

The Librarian, Culham Science Center, England

Mrs. S.A. Hutchinson, JET Library, England

Professor M.N. Bussac, Ecole Polytechnique, France

Librarian, Max-Planck-Institut für Plasmaphysik, Germany

Jolan Moldvai, Reports Library, Hungarian Academy of Sciences, Central Research Institute for Physics, Hungary

Dr. P. Kaw, Institute for Plasma Research, India

Ms. P.J. Pathak, Librarian, Institute for Plasma Research, India

Dr. Pandji Triadyaksa, Fakultas MIPA Universitas Diponegoro, Indonesia

Professor Sami Cuperman, Plasma Physics Group, Tel Aviv University, Israel

Ms. Clelia De Palo, Associazione EURATOM-ENEA, Italy

Dr. G. Grosso, Instituto di Fisica del Plasma, Italy

Librarian, Naka Fusion Research Establishment, JAERI, Japan

Library, Laboratory for Complex Energy Processes, Institute for Advanced Study, Kyoto University, Japan

Research Information Center, National Institute for Fusion Science, Japan

Dr. O. Mitarai, Kyushu Tokai University, Japan

Dr. Jiangang Li, Institute of Plasma Physics, Chinese Academy of Sciences, People's Republic of China

Professor Yuping Huo, School of Physical Science and Technology, People's Republic of China

Library, Academia Sinica, Institute of Plasma Physics, People's Republic of China

Librarian, Institute of Physics, Chinese Academy of Sciences, People's Republic of China

Dr. S. Mirnov, TRINITI, Troitsk, Russian Federation, Russia

Dr. V.S. Strelkov, Kurchatov Institute, Russian Federation, Russia

Professor Peter Lukac, Katedra Fyziky Plazmy MFF UK, Mlynska dolina F-2, Komenskeho Univerzita, SK-842 15 Bratislava, Slovakia

Dr. G.S. Lee, Korea Basic Science Institute, South Korea

Dr. Rasulkhozha S. Sharafiddinov, Theoretical Physics Division, Insitute of Nuclear Physics, Uzbekistan

Institute for Plasma Research, University of Maryland, USA

Librarian, Fusion Energy Division, Oak Ridge National Laboratory, USA

Librarian, Institute of Fusion Studies, University of Texas, USA

Librarian, Magnetic Fusion Program, Lawrence Livermore National Laboratory, USA

Library, General Atomics, USA

Plasma Physics Group, Fusion Energy Research Program, University of California at San Diego, USA

Plasma Physics Library, Columbia University, USA

Alkesh Punjabi, Center for Fusion Research and Training, Hampton University, USA

Dr. W.M. Stacey, Fusion Research Center, Georgia Institute of Technology, USA

Dr. John Willis, U.S. Department of Energy, Office of Fusion Energy Sciences, USA

Mr. Paul H. Wright, Indianapolis, Indiana, USA

The Princeton Plasma Physics Laboratory is operated
by Princeton University under contract
with the U.S. Department of Energy.

Information Services
Princeton Plasma Physics Laboratory
P.O. Box 451
Princeton, NJ 08543

Phone: 609-243-2750
Fax: 609-243-2751
e-mail: pppl_info@pppl.gov
Internet Address: http://www.pppl.gov